Acta Pharmaceutica Sinica B 2026;16(1):270−286

Chinese Pharmaceutical Association
Institute of Materia Medica, Chinese Academy of Medical Sciences

Acta Pharmaceutica Sinica B

www.elsevier.com/locate/apsb
www.sciencedirect.com

ORIGINAL ARTICLE

Palmitoylation of Tfr1 enhances platelet ferroptosis and liver injury in heat stroke

Qiyuan An[a,†], Riqing Wei[a,†], Zhicheng Huang[c], Youyong Tang[a], Minghao Wang[c], Sixiao He[d], Kaihua Huang[c], Zhifeng Liu[e,f], Meimei Zhang[g], Ru Li[a], Junhao Huang[a], Keying Zhang[a], Jingjing Ji[e,f], Liwei Xie[b,*], Qiang Ma[a,h,*]

[a]*Department of Biopharmaceutics, School of Laboratory Medicine and Biotechnology, Southern Medical University, Guangzhou 510515, China*
[b]*State Key Laboratory of Applied Microbiology Southern China, Guangdong Provincial Key Laboratory of Microbial Culture Collection and Application, Guangdong Open Laboratory of Applied Microbiology, Institute of Microbiology, Guangdong Academy of Sciences, Guangzhou 510070, China*
[c]*Department of General Surgery, Nanfang Hospital, The First School of Clinical Medicine, Southern Medical University, Guangzhou 510515, China*
[d]*School of Medicine, The Chinese University of Hong Kong, Shenzhen 518172, China*
[e]*Department of Critical Care Medicine, The Affiliated General Hospital of Southern Theatre Command of PLA, Guangzhou 510010, China*
[f]*Guangdong Branch Center, National Clinical Research Center for Geriatric Diseases (Chinese PLA General Hospital), Guangzhou 510010, China*
[g]*Department of Dermatology, Nanfang Hospital, The First School of Clinical Medicine, Southern Medical University, Guangzhou 510515, China*
[h]*The Seventh Affiliated Hospital of Southern Medical University, Foshan 528244, China*

Received 9 April 2025; received in revised form 27 August 2025; accepted 9 September 2025

KEY WORDS

Heat stroke;
Heat stroke-induced liver injury;
Platelet;

Abstract Heat stroke (HS) is a severe medical emergency characterized by coagulation and high mortality due to organ injury. This study identifies a novel mechanism in which platelet ferroptosis, driven by transferrin receptor 1 (Tfr1) palmitoylation, significantly contributes to liver injury in HS. Our findings reveal a strong inverse correlation between platelet count and organ damage, especially liver injury, as well as mortality rates. Using murine models, we demonstrate that inhibiting Tfr1-mediated ferroptosis in platelets mitigates thrombocytopenia and decreases Interleukin-1β (IL-1β) secretion, thereby

*Corresponding authors.
E-mail addresses: xielw@gdim.cn (Liwei Xie), mq@smu.edu.cn (Qiang Ma).
[†]These authors made equal contributions to this work.
Peer review under the responsibility of Chinese Pharmaceutical Association and Institute of Materia Medica, Chinese Academy of Medical Sciences.

https://doi.org/10.1016/j.apsb.2025.10.027
2211-3835 © 2025 The Authors. Published by Elsevier B.V. on behalf of Chinese Pharmaceutical Association and Institute of Materia Medica, Chinese Academy of Medical Sciences. This is an open access article under the CC BY-NC-ND license (http://creativecommons.org/licenses/by-nc-nd/4.0/).

Ferroptosis;
Tfr1;
Palmitoylation;
Cytokines;
IL-1β

improving liver function and survival outcomes. This research highlights Tfr1 palmitoylation as a critical factor in iron transport within platelets, with the palmitoylation inhibitor 2-bromopalmitate (2BP) effectively reducing total iron, Fe^{2+}, lipid ROS, 4-hydroxynonenal (4-HNE), and cell cytotoxicity under heat stress. These results suggest that targeting Tfr1 palmitoylation-dependent ferroptosis in platelets offers a novel therapeutic strategy for treating HS-induced thrombocytopenia and liver injury.

© 2025 The Authors. Published by Elsevier B.V. on behalf of Chinese Pharmaceutical Association and Institute of Materia Medica, Chinese Academy of Medical Sciences. This is an open access article under the CC BY-NC-ND license (http://creativecommons.org/licenses/by-nc-nd/4.0/).

1. Introduction

Heat stroke (HS) is emerging as a leading global health challenge, particularly with the ongoing trend of global warming. HS frequently leads to systemic inflammatory response syndrome and multi-organ system failure or multi-organ dysfunction syndrome, driving its high mortality rate[1]. A critical complication of HS is liver injury, which often escalates to acute liver failure (ALF)[1]. Current treatments, including liver transplantation and systemic support, lack specificity, highlighting the requirement for targeted therapeutic strategies and a deeper understanding of the molecular mechanisms driving HS-induced liver injury.

Abnormal and excessive immune responses, caused by damage-associated molecular patterns (DAMPs) and intestinal endotoxin, are hallmarks of HS liver damage[1]. These endotoxins, primarily cleared by liver-resident macrophages (Kupffer cells), trigger a significant immune response[2]. The contribution of monocyte-derived macrophages and dendritic cells in liver tissue is also notable, especially in iron and cholesterol metabolism and antigen presentation[2]. Platelets, known to play a critical role in bacterial clearance and systemic inflammatory response in various liver injury models, have an unexplored role in HS-induced liver injury[3,4]. Particularly, the mechanisms underlying HS-induced thrombocytopenia and the role of platelets in ALF, where serum thrombopoietin (TPO) levels are inconsistently altered, are not well-understood[5,6].

HS-induced liver injury is characterized by hepatocyte degeneration and diverse cell death pathways, including pyroptosis, necrosis, apoptosis, and mitophagy[7]. Notably, heat shock transcription factor 1 is linked to cell death through the receptor-interacting protein kinase 3-dependent activation of Z-DNA binding protein 1[8]. Additionally, excessive reactive oxygen species (ROS) production during heat stress can activate the Nlrp3 inflammasome and pyroptosis, thereby exacerbating hepatocyte death[9]. Moreover, impaired mitophagy, due to interaction between p53 and Parkin, leads to increased ROS and apoptosis[10]. Furthermore, high ROS levels are linked to susceptibility to ferroptosis, a regulated cell death intrinsically linked to iron metabolism[11]. Iron not only catalyzes lipoxygenases, cytochrome P450 oxidoreductase, and other metabolic enzymes involved in phospholipid peroxidation and the production of cellular ROS, but it is also essential for the non-enzymatic, iron-dependent Fenton reaction[11].

Iron is an essential element for DNA synthesis and energy metabolism. However, in heat stroke, high temperature causes cell damage and hemolysis, releases a large amount of free iron, activates the Fenton reaction, produces a large amount of ROS, and aggravates oxidative stress[12]. Transferrin receptor 1 (Tfr1), a transmembrane glycoprotein, serves as the primary receptor for cellular iron metabolism by mediating the transport of transferrin-bound ferric ions into cells[13]. The endocytosis and degradation of Tfr1 directly regulate cellular iron uptake and metabolism, processes that are closely linked to ferroptosis[14,15]. The dynamic trafficking of Tfr1 has been reported to be regulated by palmitoylation, a post-translational lipid modification[15-17]. Palmitoylation involves the attachment of palmitic acid to proteins mediated by a family of *S*-acyltransferases that contain a conserved aspartate−histidine−histidine−cysteine (DHHC) cysteine-rich domain, which occurs dynamically and reversibly, acting as a molecular on/off switch[18]. Alterations in palmitoylation and deacylation dynamics are associated with a range of disorders and diseases[18]. Emerging evidence indicates that dysregulated metabolic pathways and impaired iron homeostasis have been implicated in the progression of acute and chronic liver diseases *via* ferroptosis[14]. However, the specific role of ferroptosis in HS-induced liver injury requires additional investigation.

In this study, we demonstrate that platelet ferroptosis mediated by a Tfr1 palmitoylation-dependent mechanism is a key contributor to liver injury in a murine HS model, revealing the potential role of Tfr1 palmitoylation as a novel therapeutic target for HS-induced thrombocytopenia and liver injury.

2. Materials and methods

2.1. Clinical study design, participants and analysis

This observational study included 189 adult patients with severe HS, admitted to the ICU of the General Hospital of Southern Theater Command, Guangzhou, China, from October 2008 to May 2019. A healthy control (HC) group of 183 adults was recruited from the Seventh Affiliated Hospital of Southern Medical University, Foshan, China, between May 2020 and September 2023. Ethical approval was granted by the Institutional Review Board of the Medical Ethics Committee (Permission No. HE-2020-09, 2025-0026), adhering to the Declaration of Helsinki. Written consent was waived by the Ethics Committee. Severe heat stroke was defined as an acute heat-induced illness with hyperthermia (core temperature above 40 °C) and neurological dysfunction following exposure to hot and humid conditions, with or without strenuous physical exertion[19]. Pregnant or nursing women and individuals with life-threatening comorbidities were excluded. Patients received standard supportive care upon admission. Clinical data and organ function parameters were collected at admission and 24 h post-admission. Organ dysfunctions were defined as follows: thrombocytopenia (platelet counts $<100 \times 10^9$/L), central nervous system (Glasgow coma scale (GCS) ≤ 8), heart injury (cardiac troponin I (CTNI) > 100 pg/mL), liver injury (alanine aminotransferase (ALT) > 50 U/L), and kidney (serum creatinine (CR) > 106 μmol/L). Survival time was monitored up to 90 days. Bioinformatic analyses of the clinical data, including principal component analysis with examination of loadings on the first

principal component, and correlation matrix heatmap generation, were performed using R software. Prior to principal component analysis and heatmap visualization, missing values were imputed for each variable. Pairwise Spearman or Pearson correlations were calculated in GraphPad Prism, excluding missing values.

2.2. Animal models

All animal studies were approved by the Nanfang Hospital of Southern Medical University review board (Permission No. IACUC-LAC-20230411-006) and aligned with NIH guidelines. SPF mice were sourced from the Southern Medical University Animal Center, Guangzhou, China. *PF4-Cre* mice were acquired from Cyagen Biosciences (Stock number C001050), and *Tfr1*$^{fl/fl}$ mice from Jackson Laboratory (Strain number 028363) were provided by Professor Liwei Xie[20,21]. Mice with *Tfr1*-specific deletion in the platelet were generated by crossing mice carrying *PF4-Cre* and *Tfr1*$^{fl/fl}$ alleles (referred to as CKO-*Tfr1*). All experimental animals were housed under a controlled specific pathogen-free environment (12 h light/dark cycle, 25 °C ambient temperature, 55 ± 5% relative humidity) with free access to standard chow and water. The thrombocythemia mouse model was induced by TPO injections (i.p., 1100 U/kg, 7 days, 3SBIOINC, Shenyang, China), while thrombocytopenia was induced using mouse platelet depletion antibodies (i.v., 2000 μg/kg, R300, emfret Analytics, Eibelstadt, Germany). AAV9-CMV-DIO-*Tfr1* (referred to as AAV9-DIO-*Tfr1*) virus was produced using a standard triple transfection system, collected and concentrated[22]. For the Tfr1 rescue experiment in CKO-*Tfr1* mice, AAV9-DIO-*Tfr1* was injected *in vivo* (5×10^{11} vg) to induce *Tfr1* overexpression. Drug treatments, including ferrostatin-1 (fer-1, i.p., 10 mg/kg, S7243, Selleckchem, Houston, TX, USA), deferoxamine mesylate (DFO, i.p., 20 mg/kg, bid, 7 days, D9533, Sigma−Aldrich, St. Louis, MO, USA), were administered prior to model establishment. Male mice (8−10 weeks) were weighed prior to model establishment, and food and water were withheld. Sham heat rest (SHR) mice were kept in cages at 25 °C ambient temperature and 55% relative humidity. To establish the HS model, mice were placed under specific conditions (39.5 °C, 65% relative humidity) in a climate chamber (ARQ-250, GEMTOP Scientific Instrument, Shanghai, China), with rectal temperature monitored. Mice were immediately removed from the climate chamber post-HS, weighed, returned to their normal feeding environment, and given ad libitum access to food and water.

2.3. Weight alteration

Weight alteration of each mouse was calculated using Eq. (1):

$$\text{Weight alteration (\%)} = (\text{Weight prior to heat stress} - \text{Weight at Tc, max})/\text{Weight prior to heat stress} \times 100 \quad (1)$$

The SHR groups underwent the same procedure without being heated.

2.4. Sample collection and analysis

Blood samples from mice were collected post-anesthesia using sodium pentobarbital (50 mg/kg, i.p.). Complete blood counts were analyzed by an Automated Hematology Analyzer (BC-2800vet, Mindray, Shenzhen, China). Biochemical parameters were measured by an Automatic Chemistry Analyzer (8021A, URIT, Guilin, China).

2.5. Haematoxylin and eosin (HE) staining

Tissue sections at 4 μm were stained with HE solution. For staining, the sections were first incubated at 60 °C for 2 h to melt the paraffin, followed by deparaffinization (2 rinses in xylene, 15 min each) and rehydration (2 rinses in 100% alcohol, followed by 95%, 85%, 75% alcohol and pure water for 5 min each). The sections were performed following the standard HE protocol and fixed with neutral balata subsequently. Images were captured by an EVOS FL auto fluorescent microscope (Thermo Fisher Scientific, Waltham, MA, USA).

2.6. Platelet purification and treatment

The sodium citrate anticoagulated whole blood was diluted with 0.9% normal saline containing prostaglandin E1 (final concentration 1 μmol/L) and subsequently centrifuged (150 × *g*, 10 min) to collect platelet-rich plasma. Then, the platelet-rich plasma was centrifuged (750 × *g*, 10 min), and platelet pellets were resuspended in autoMACS Rinsing Solution containing 0.5% bovine serum albumin (BSA) and 1 μmol/L prostaglandin E1 (900100P, AvantiResearch, Alabaster, AL, USA) and passed through an Acrodisc white blood cell (WBC) Syringe Filter (AP-4951, Pall Corporation, Port Washington, NY, USA). Each platelet filtrate was incubated with anti-CD45 beads (130-052-301, Miltenyi Biotec, Bergisch Gladbach, Germany) and anti-Ter-119 beads (130-049-901, Miltenyi Biotec) according to the manufacturer's instructions and using LD MidiMACS Starting Kit (130-090-329, Miltenyi Biotec, Bergisch Gladbach, Germany) to remove residual leukocytes and red blood cells (RBC), respectively. The purified platelets were obtained and then washed in Rinsing Solution with prostaglandin E1 prior to processing. For drug treatment, the purified platelets were pretreated with DFO (100 μmol/L), fer-1 (5 μmol/L), Trolox (100 μmol/L, S3665, Selleckchem, Houston, TX, USA), 2-bromopalmitate (2BP, 5 μmol/L, 238422, Sigma−Aldrich), staurosporine (0.3 μmol/L, HY-15141, MedChemExpress, Monmouth Junction, NJ, USA), benzyl-α-GalNAc (1 mmol/L, HY-129389, MedChemExpress), tunicamycin (2 μg/mL, HY-A0098, MedChemExpress) for 1 h before heat stress. Platelets were co-cultured with AML12 (ATCC, Manassas, VA, USA) or mouse Kupffer cells, with or without ferroptosis inhibitors, to facilitate subsequent relevant experiments.

2.7. RNA-seq and bioinformatic analysis

The purified platelet pellet was dissolved in TRIzol and stored at −80 °C until RNA isolation. RNA was purified from platelets according to the manufacturer's protocol and resuspended in RNAse-free dH_2O. The concentration and integrity of RNA were assessed using the RNA Nano 6000 Assay Kit of the Bioanalyzer 2100 system (Agilent Technologies, CA, USA) in the Novogene Co., Ltd. Poly(A)-tailed mRNA was prepared from total RNA and sequenced by the Illumina NovaSeq 6000 (San Diego, CA, USA) subsequently. The image data, measured by the high-throughput sequencer, was converted into sequence data (raw data) by CASAVA base recognition. Clean data, obtained from raw data by removing low-quality reads and reads containing adapters and Nbase, were used for downstream analysis, referenced to the mouse genome and gene model annotation from the

genome website. Bioinformatic analyses were performed as previously described[23,24].

2.8. Transmission electron microscopy (TEM) and immunoelectron microscopy (IEM)

Ultrastructural changes were examined using TEM and IEM. Isolated samples were fixed with 2.5% phosphate-glutaraldehyde. For TEM, images were acquired with JEOL JEM-1400 plus (Akishima, Tokyo, Japan) and Hitachi H-7500 (Chiyoda-ku, Tokyo, Japan) transmission electron microscopes. For IEM, the fixed samples were incubated with anti-Tfr1 monoclonal antibody at a dilution of 1:250 and 10 nm affinity-isolated colloidal gold secondary antibody for immunogold staining. Images were acquired with a Hitachi HT-7800 (Chiyoda-ku, Tokyo, Japan) transmission electron microscope.

2.9. Iron assay

Intracellular total iron levels were measured by total iron content colorimetric assay kit (E1042, Applygen, Beijing, China) according to the instructions. Briefly, clean samples were lysed with 200 μL lysis buffer in a shaker for 2 h. The buffer mixed with 4.5% potassium permanganate solution proportionally, which is called mixture A. Mix samples with Mixture A in equal proportions and incubate them at 60 °C for 1 h, add iron ion detection reagent, then incubate at room temperature for 30 min. Samples were read at 550 nm, and the concentration of unknown samples was calculated with reference to the standard curve. Fe^{2+} of cells was assessed using the commercially available FerroOrange (F374, Dojindo, Kamimashiki-gun, Kumamoto, Japan) following the manufacturer's guidelines. In brief, the treated samples were exposed to 1 μmol/L FerroOrange with HBSS and allowed to incubate at 37 °C for 20 min, and then subjected to analysis using flow cytometry.

2.10. Enzyme-linked immunosorbent assay

Coagulative factors, interleukin-1β (IL-1β) and lipid peroxidation metabolites were measured by enzyme-linked immunosorbent assay in accordance with the manufacturer's instructions, respectively: IL-1β (CSB-E08054m/E08053h, CUSABIO, Wuhan, China), IL-6 (CSB-E04639m, CUSABIO), IL-10 (CSB-E04594m-IS, CUSABIO), TNF-α (CSB-E04741m, CUSABIO) and 4-hydroxynonenal (4-HNE, CSB-E13412m/E16214h, CUSABIO).

2.11. Flow cytometry

The level of lipid ROS (C11-BODIPY581/591, D3861, Invitrogen, Carlsbad, CA, USA), ROS (H2DCFDA, Redox-Sensitive Probe, HY-D0940, MedChemExpress), Tfr1 (113807, Biolegend, San Diego, CA, USA; 561939, BD Biosciences, Franklin Lakes, NJ, USA), Caspase-1 (97/9122, ImmunoChemistry, Bloomington, MN, USA), CD61 (104306, Biolegend), CD42b (303903, Biolegend), CD62p (148304, Biolegend) in platelets, and PI staining for AML12, were measured by a CytoFLEXS flow cytometer (BECKMAN Coulter, Fullerton, CA, USA) according to manufacturer instructions respectively and the data were analyzed by FlowJo-V10 software.

2.12. Quantitative real-time PCR

Purified total RNA was used for complementary DNA synthesis using SweScript All-in-One RT SuperMix for qPCR (One-Step gDNA Remover, G3337, Servicebio, Wuhan, China), followed by the 2 × Universal Blue SYBR Green qPCR and Master Mix (G3326, Servicebio) to assess mRNA expression levels, referred to the instructions.

2.13. Western blot and co-immunoprecipitation (co-IP) analysis

Total proteins extracted from samples were subjected to SDS-PAGE gel electrophoresis. After being transferred to polyvinylidene fluoride membranes, anti-Tfr1 (ab214039, Abcam, Cambridge, United Kingdom), anti-zinc finger DHHC-type containing protein 2 (ZDHHC2, PA5101994, Invitrogen), and β-Tubulin were incubated at 4 °C overnight. The membranes were washed with Tris-buffered saline containing 0.1% Tween-20, and then incubated with secondary antibodies at room temperature for 2 h. Target bands were visualized with enhanced chemiluminescent reagents.

For co-IP, cells were harvested and lysed in lysis buffer. Then, lysates were subjected to immunoprecipitation with anti-Tfr1 antibody or Rabbit IgG according to the instructions. Add the protein−antibody complex to protein A/G magnetic beads and incubate overnight at 4 °C. Immune complexes were washed and subjected to immunoblotting.

2.14. Cell culture and stable cell line establishment

MEG-01 cells (ATCC) were grown at 37 °C in 5% CO_2 in RPMI-1640 containing 10% FBS and 1% penicillin−streptomycin. *Tfr1*-overexpression lentivirus and shRNA lentiviruses specific to the target genes were used for stable cell line generation. The plasmid and the packaging vectors were co-transfected into HEK293T cells (ATCC), and the virus-containing supernatant was collected 48 h later. The cells to be infected were incubated with the virus-containing supernatant with 6 μg/mL polybrene for 48 h and then selected with 2 μg/mL puromycin.

2.15. Preparation of platelet-like particle (PLP)

For maturation and differentiation, MEG-01 cells were treated with 2.5 mmol/L valproic acid (HY-10585, MedChemExpress) for 9 days. Subsequently, PLP production was stimulated by rhTPO (100 ng/mL, 96-300-18-10, PeproTech, Cranbury, NJ, USA) for 72 h. To isolate PLP, the culture medium was centrifuged at 100 × *g* for 10 min to remove the nucleated cells. Supernatant was then centrifuged at 750 × *g* for 10 min at room temperature to isolate PLP, and the pellet containing PLP was resuspended in culture medium. To activate PLP or platelets, arachidonic acid (AA, 0.3 mmol/L, 10931, Sigma−Aldrich) or Adenosine 5′-diphosphate (ADP, 1 μmol/L, HY-W010918, MedChemExpress) was added to the suspension for 5 min.

2.16. Wright-giemsa stain

Suspension cells or PLPs were initially washed and spread on poly-L-lysine hydrobromide (P1399, Sigma−Aldrich) coated slides. After being fixed in methanol for 15 min, samples were stained in Wright-Giemsa solution for 5 min, washed with PBS

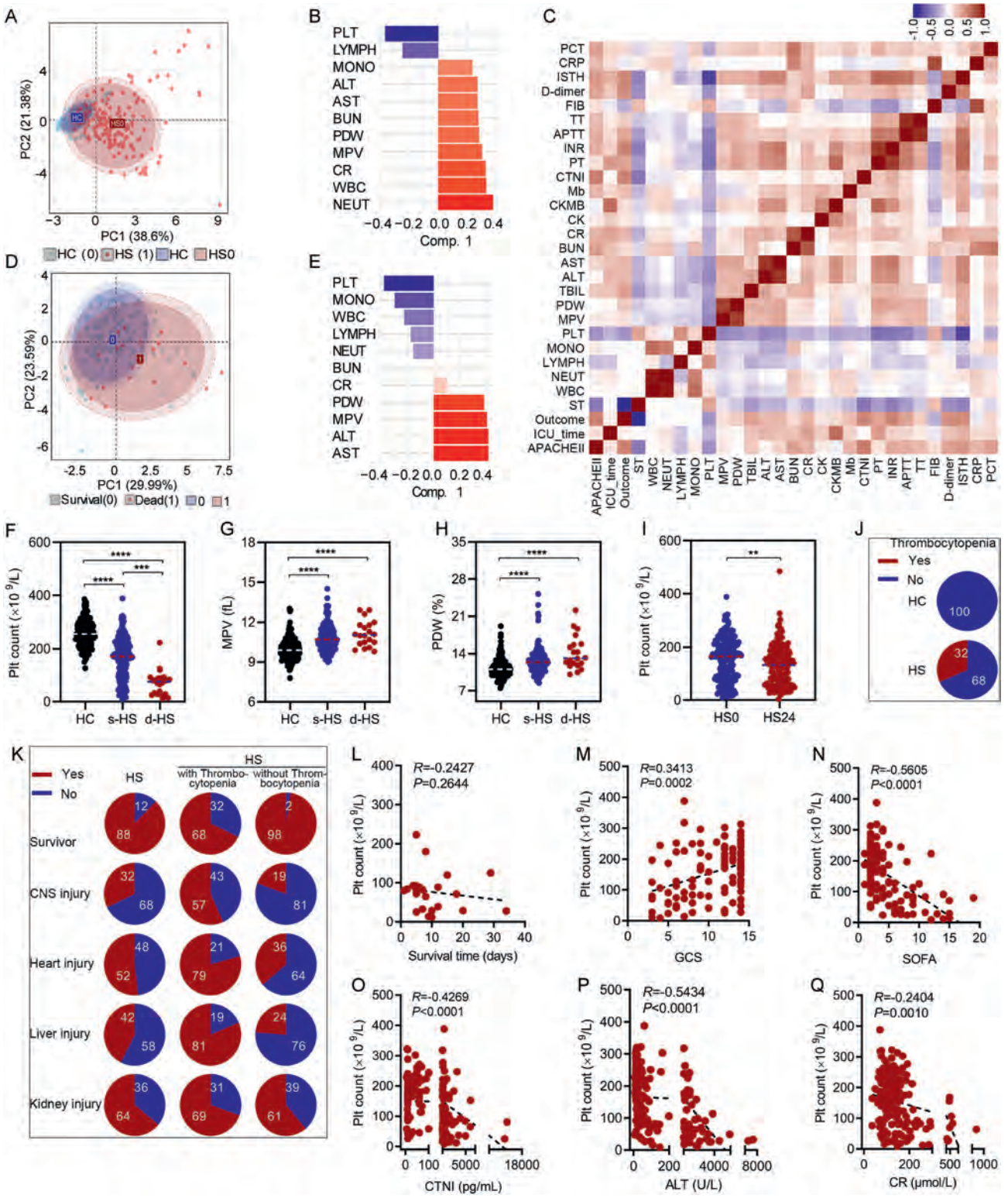

Figure 1 Admission platelet counts are associated with poor survival rates and severe liver injury in the heat stroke (HS) cohort. (A) Principal Component Analysis (PCA) distinguishes between healthy control (HC, $n = 183$) and HS ($n = 189$) at the time of admission. (B) Loadings on principal component 1 (PC1) represent contributions of each factor in panel A. (C) Correlation matrix heatmap between routine blood indicators and multiple organ damage indicators at the time of admission. (D) Survivor HS (s-HS, $n = 166$) and deceased patients (d-HS, $n = 23$) were separated by PCA at the time of admission. (E) Loadings on PC1 represent contributions of each factor in panel D. (F–H) Scatter plots showing admission levels of platelet count (F), mean platelet volume (MPV) (G), and platelet distribution width (PDW) (H) in HC, s-HS, and d-HS groups (platelet count: HC, $n = 182$; s-HS, $n = 164$; d-HS, $n = 22$; MPV and PDW: HC, $n = 182$; s-HS, $n = 155$; d-HS, $n = 20$). Horizontal lines indicate the medians. Missing values were excluded. (I) Scatter plots showing platelet counts at 0 h ($n = 186$) and 24 h ($n = 187$) post-admission. Horizontal lines indicate the medians. Missing values were excluded. (J) Pie charts showing thrombocytopenia (platelet counts $<100 \times 10^9$/L) in

buffer and pure water, and observed by EVOS FL auto fluorescent microscope.

2.17. Simulated HS model in vitro

The cells, platelets, or PLPs were exposed to heat stress at 43 °C for 2 h in a humidified cell culture incubator, then transferred to a normal incubator and maintained at 37 °C with 5% CO_2 for recovery over different time points.

2.18. Cytotoxicity assay

Cellular supernatants at SHR and different time points after heat stress were collected, and the LDH Cytotoxicity Assay Kit (C0017, Beyotime Biotechnology, Shanghai, China) was used to test the cell cytotoxicity according to the manufacturer's instructions. Using a microplate reader to detect optical density values at 490 nm. PI staining, performed according to the instructions and detected by flow cytometry, was also used to evaluate cell cytotoxicity.

2.19. Immunofluorescence and immunohistochemistry

Tissue sections were deparaffinized and rehydrated as above. Using EDTA Antigen Retrieval Solution (pH = 9.0) for antigen retrieval, 3% H_2O_2 to eliminate endogenous peroxidase, and 5% BSA to block non-specific antigens. After blocking, Clec4f (AF2784, R&D Systems, Minneapolis, MN, USA), Glutamine Synthetase (ab73593, Abcam), CD42b (ab183345, Abcam) were incubated at 4 °C overnight. For cellular immunofluorescence, sections were first fixed with 4% paraformaldehyde at room temperature for 30 min, followed by permeabilization with 0.25% Triton X-100 for 15 min, and then blocked to prevent non-specific binding. Platelets were stained with CellTracker Green CMFDA (C7025, Invitrogen) at 37 °C for 30 min. Primary antibodies were incubated at 4 °C overnight. Subsequently, the slides were incubated with peroxidase-labeled goat anti-rabbit IgG polymer or goat anti-mouse IgG polymer for 30 min at room temperature. A tyramide signal amplification indirect kit (DFT4C100, HISTOVA, Beijing, China) was used according to the manufacturer's instructions to boost and detect the signal.

For immunohistochemistry, Ki-67 (GB111141, Servicebio) was incubated overnight at 4 °C. The sections were then washed and treated with goat anti-rabbit IgG polymer for 30 min at room temperature. Following this, the slides were incubated with DAB substrate solution (8059, Cell Signaling Technology, Danvers, MA, USA) until the color developed. Images were captured and visualized by EVOS FL Auto fluorescence microscope or laser scanning confocal microscope (Zeiss LSM880, Leica, Wetzlar, Germany), and analyzed with ZEN microscopy software.

2.20. Acyl-biotin exchange (ABE) palmitoylation assay

The samples were lysed using lysis buffer supplemented with protease inhibitor. Subsequently, 50 mmol/L *N*-ethylmaleimide (23030, Thermo Fisher Scientific) was added to the lysis to alkylate free cysteine residues. The palmitoyl thioester bond was then hydrolysed using 1 mol/L hydroxylamine (26103, Thermo Fisher Scientific) and replaced with HPDP-Biotin. The cell lysates were then coupled with streptavidin beads (LSKMAGT02, Millipore, Burlington, MA, USA) at room temperature for 1 h. Ultimately, palmitoylated Tfr1 was identified by immunoblotting alongside the control group without hydroxylamine treatment.

2.21. TF-Tfr1 internalization and recycling

PLPs were starved in FBS-free 1640 media for 1 h prior to heat stress and collected after heat stress. Subsequently, samples were placed on ice for 10 min, washed with cold live cell imaging solution containing 20 mmol/L glucose and 1% BSA, and incubated with Alexa Fluor 488-conjugated transferrin (holo-TF, T13342, Invitrogen) for 5 min at 37 °C, followed by three washes. Mean fluorescence intensity of holo-TF on the Alexa 488 channel was used to reflect Tfr1 internalization and recycling.

2.22. Statistical analysis

The results were presented as mean ± standard error of mean (SEM) unless otherwise stated. Statistical analyses were performed using GraphPad Prism using Student's *t*-test or one/two-way ANOVA. Pairwise correlations were assessed using Spearman's or Pearson's correlation. Kaplan−Meier survival curves analysis was calculated by the log-rank (Mantel-Cox) test. Values of $P < 0.05$ were considered significant.

3. Results

3.1. Association of platelet counts with survival and liver injury in heat stroke patients

Our previous work showed that admission platelet count is associated with 90-day mortality in HS patients[19]. However, the differences between HC and HS, as well as the dynamic changes in platelet count and the strength of the correlation between damage to various organs and the most platelet-affected organ in HS, have not been fully recognized. Significant differences were found between HC ($n = 183$) and HS patients ($n = 189$), as well as deceased patients (d-HS) and survivors (s-HS) (Fig. 1A, B, D and E, Supporting Information Fig. S2A, S2B, S2D and S2E). Platelet counts were identified as a critical factor correlated with organ injury in HS (Fig. 1C, Fig. S2C). HS patients, particularly d-HS,

the HC ($n = 182$) and admission HS groups ($n = 186$). Missing values were excluded. (K) Pie charts implying admission mortality and complications in the HS groups (HS with thrombocytopenia, $n = 59$; HS without thrombocytopenia, $n = 127$). Missing values were excluded. (L−Q) Admission correlation between platelet counts and survival time (L) (in dHS, $n = 23$), Glasgow coma scale (GCS) scores (M) ($n = 114$), sequential organ failure assessment (SOFA) (N) ($n = 114$), CTNI (O) ($n = 160$), ALT (P) ($n = 185$), and CR (Q) ($n = 185$). Missing values were excluded. $^{**}P < 0.01$, $^{***}P < 0.001$, $^{****}P < 0.0001$. PLT: platelet counts; LYMPH: lymphocytes; MONO: monocytes; ALT: alanine aminotransferase; AST: aspartate aminotransferase; BUN: blood urea nitrogen; PDW: platelet distribution widths; MPV: mean platelet volumes; CR: serum creatinine; WBC: white blood cell; NEUT: neutrophils; PCT: procalcitonin; CRP: C-reactive protein; ISTH: International Society on Thrombosis and Haemostasis DIC score; FIB: fibrinogen; TT: Thrombin time; APTT: activated partial thromboplastin time; INR: international normalized ratio; PT: prothrombin time; CTNI: cardiac troponin I; Mb: myoglobin; CKMB: creatine kinase MB isoenzyme; CK: creatine kinase; TBIL: total bilirubin; ST: survival times; APACHE II: acute physiology and chronic health evaluation II score.

had significantly lower platelet counts than HC (Fig. 1F). Notably, d-HS patients and those 24 h post-admission displayed larger mean platelet volumes (MPV) and wider platelet distribution widths (PDW), indicating the prevalence of young and active platelets (Fig. 1G and H, Supporting Information Fig. S1A and S1B). Post-admission analysis showed a marked decline in platelet counts, indicating escalating thrombocytopenia (platelet counts $<100 \times 10^9$/L) in HS patients (Fig. 1I). Thrombocytopenia was found in 32% of HS patients, associated with severe complications and higher mortality upon admission (Fig. 1J and K). Compared to HC, levels of aspartate aminotransferase (AST) (Fig. S1C), ALT (Fig. S1D), and serum CR (Fig. S1E) were elevated in d-HS patients. Correlation analysis revealed a moderate positive association between platelet counts and GCS (Fig. 1M), and a moderate to strong negative correlation with sequential organ failure assessment (SOFA), CTNI, ALT, AST, total bilirubin (TBIL), and acute physiology and chronic health evaluation II (APACHE II) scores both on admission and 24 h post-admission (Fig. 1L−Q, Figs. S1F−S1H and S2). Additionally, the liver was the most affected organ by platelet count (Fig. 1K−Q, Fig. S1F−S1H). MPV and PDW were slightly positively associated with liver damage (Figs. S1 and S2). Shifts in WBC counts and subtypes (neutrophils (NEUT), monocytes (MONO), and lymphocytes (LYMPH)) exhibited a trend towards baseline levels 24 h post-admission (Supporting Information Fig. S3). Correlation analysis also identified WBC counts and subtypes as potentially relevant to organ injury and mortality, although the correlation was limited and may have been influenced by therapeutic care upon admission (Fig. 1C, Fig. S2C, Supporting Information Figs. S4 and S5). These findings underscore the critical association of platelet count with organ damage, especially liver injury, in HS patients, suggesting it may as an effective factor for therapeutic intervention.

3.2. *Platelets participate in liver injury of the HS murine model*

To explore the role of platelets in HS and HS-induced liver injury, mice were subjected to heat stress, which resulted in a triphasic core temperature (Tc) pattern with significant weight loss and dehydration (Fig. 2A, Supporting Information Fig. S6A and S6B). Platelet counts decreased notably at 0, 6, and 24 h post-HS (Fig. 2B). LDH cytotoxicity assays revealed increased platelet mortality under heat stress *in vitro* (Fig. 2C), indicating a direct thermal impact on platelet viability. RBC (Fig. S6C) and WBC (Fig. S6D) counts exhibited distinct patterns post-HS. While LDH cytotoxicity assays on these cells and megakaryocyte cell lines (MEG-01) under heat stress *in vitro* showed only marginal changes (Fig. S6E−S6I), indicating specific platelet vulnerability. Liver histopathology (Fig. S6J) and plasma ALT, AST (Fig. 2D and E) revealed extensive liver damage, which is consistent with the increased systemic inflammation marker IL-1β levels post-HS onset (Fig. 2F). Correlation analysis revealed significant negative associations between platelet counts and the core temperature at HS onset (HS0) (Fig. 2G), ALT (Fig. 2H), and IL-1β (Fig. 2I), implicating the role of platelet counts in HS and HS-related liver injury. Modulating platelet counts using TPO and mouse platelet depletion antibodies (αCD42b) affected ALT levels and liver histology, further highlighting the pivotal role of platelets in liver injury (Fig. 2J−L). *In vitro*, co-culture experiments with AML12 hepatocytes and platelets corroborated the detrimental role of platelets in HS-induced liver injury (Supporting Information Figs. S6K and S7K). This study elucidates the critical role of platelets in mediating liver injury during heat stroke, providing valuable insights for potential therapeutic interventions in HS management.

3.3. *Ferroptosis-induced platelet decline in the HS murine model*

To investigate the mechanisms driving platelet count reduction in HS, we analyzed RNA sequencing data from platelets collected at various time points post-HS (0, 6, 24 h) in mice. A heatmap showing differentially expressed genes at 0, 6, 24 h post-HS relative to the SHR group (Fig. 3A). GO analysis highlighted several upregulated pathways associated with iron metabolism and lipid peroxidation in the HS group (Fig. 3B, Fig. S7A−S7D), which was further validated by Gene Set Enrichment Analysis, as ferroptosis (Fig. 3C). TEM analysis revealed mitochondrial morphological changes indicative of ferroptosis in platelets, including volume shrinkage and increased membrane density (Fig. 3D). Iron assays revealed that total iron and Fe^{2+} levels were markedly increased post-HS (Fig. 3E, Fig. S7E and S7F). Additionally, the levels of 4-HNE, a marker of lipid peroxidation, were also significantly elevated post-HS (Fig. 3F). The accumulation of total ROS and lipid ROS was assessed both *in vivo* (Fig. 3G−J) and *in vitro* (Fig. S7G−S7J), confirming ferroptosis as a key mediator of platelet death in HS. Pretreatment with ferroptosis inhibitors effectively reduced lipid ROS (both *in vivo* and *in vitro*) and LDH cytotoxicity (*in vitro*), highlighting the pivotal role of ferroptosis in HS-induced platelet decline (Fig. 3K−M). Furthermore, the ferroptosis inhibitor significantly reduced hepatocyte mortality when platelets were co-cultured with AML12 hepatocytes *in vitro* (Fig. S7K). These findings underscore ferroptosis as a crucial mechanism in platelet reduction during HS, drawing attention to this iron-mediated cell death pathway characterized by iron-dependency and lipid peroxidation in HS.

3.4. *Tfr1 palmitoylation drives ferroptosis in platelets during HS*

To identify potential candidate genes involved in platelet ferroptosis, mRNA expression profiles related to ferroptosis were analyzed. Interestingly, several iron homeostasis-related genes showed altered expression post-HS, along with changes in other ferroptosis-associated genes (Fig. 4A). Notably, the expression levels of *Tfr1*, *Hmox1*, *Steap3*, *Ptgs2*, *Hspb1*, and *Slc40a1* were markedly elevated post-HS (Fig. 4B, Fig. S7L). To investigate the role of these genes in platelet ferroptosis, PLPs derived from MEG-01 cells were used *in vitro*. The structure and function of these PLPs resembled platelets (Supporting Information Fig. S8). Lentivirus was used to interfere with the expression of target genes in MEG-01 cells and PLPs (Supporting Information Fig. S9A). It was found that sh-*Tfr1* most significantly reduced total iron (Fig. S9B), Fe^{2+} (Fig. S9C), lipid ROS (Fig. S9D), 4-HNE (Fig. S9E), and mortality (Fig. S9F) in PLPs under heat stress *in vitro*. Tfr1 is the rate-limiting factor that controls iron uptake and drives the process of ferroptosis[11], suggesting that Tfr1 may also play an important role in heat stress-induced ferroptosis in platelets. The results showed that the expression of Tfr1 protein in platelets increased post-HS (Fig. 4C and D). CKO-*Tfr1* mice were used to decrease the expression of *Tfr1* in platelets (Fig. 4E and F). *Tfr1* ablation in platelets increased resistance to the decline in platelet count (Fig. 4G) and also reduced total iron (Fig. 4H), Fe^{2+} (Fig. S9G), lipid ROS (Fig. 4I) and 4-HNE (Fig. 4J) induced by HS *in vivo*, as well as platelet mortality *in vitro* (Fig. 4K),

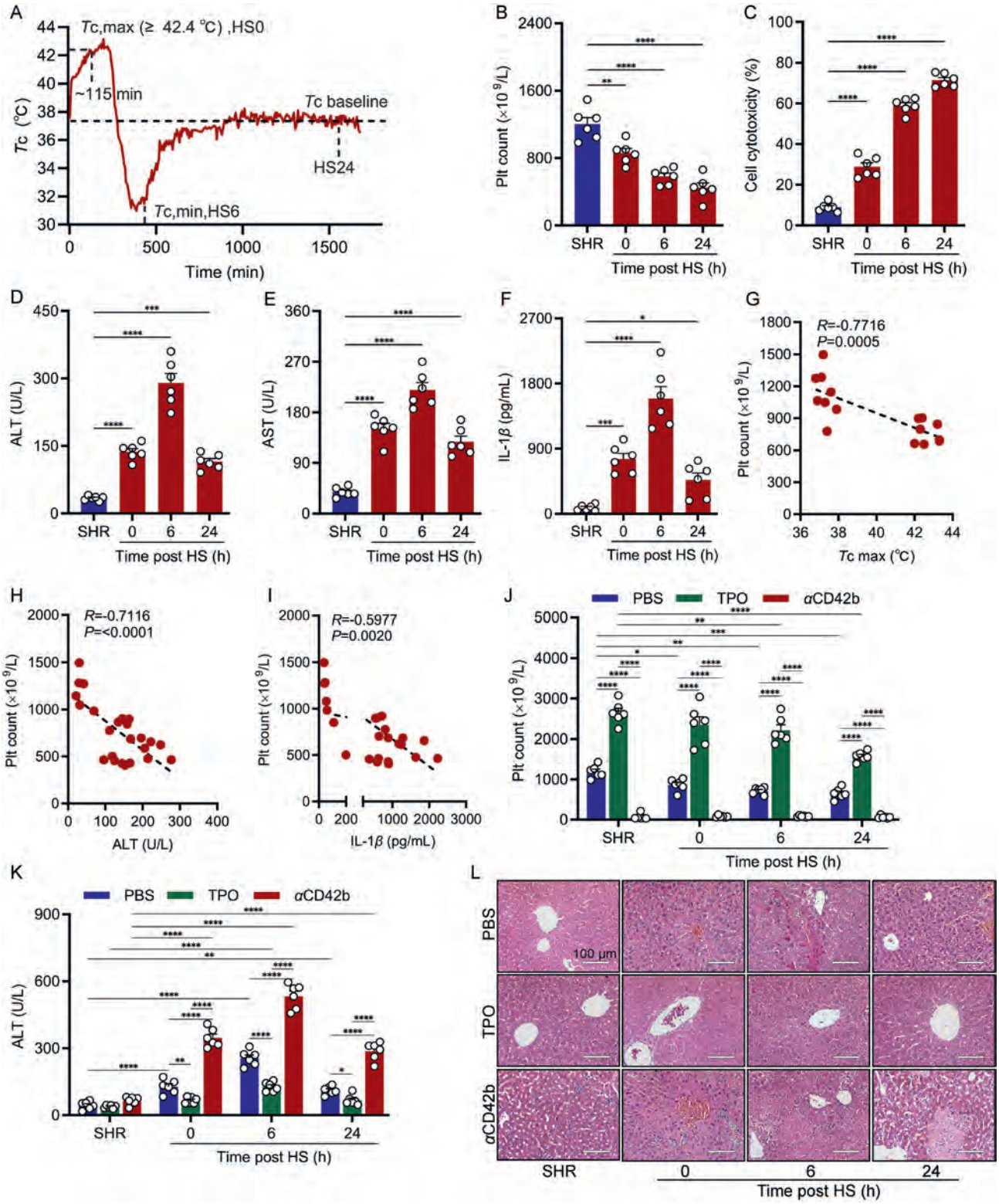

Figure 2 Platelets participate in liver injury in the HS murine model. (A) Thermoregulatory graphical description of heat stress profile aspects within 28 h in mice (shown as mean only, total $n = 25$). (B) Platelet counts along the time axis at sham heat rest (SHR) and 0, 6, 24 h post-HS ($n = 6$ mice per group). (C) Cell cytotoxicity of mouse platelets was measured by LDH activity under heat stress *in vitro* ($n = 6$ mice per group). (D−F) Plasma ALT (D) and AST (E) and IL-1β (F) levels in SHR mice and mice at 0, 6, 24 h post-HS ($n = 6$ mice per group). (G−I) Correlation between platelet counts and Tc max at HS onset ($n = 16$), ALT ($n = 24$), and IL-1β ($n = 24$) levels. (J−L) Blood platelet counts (J), plasma ALT levels (K), and representative HE staining images of liver tissue (L) were assessed in SHR mice and mice at 0, 6, 24 h post-HS, with or without pretreatment with the platelet-depleting antibody αCD42b or the platelet stimulator thrombopoietin (TPO) ($n = 6$ mice per group, scale bars: 100 μm). Mean ± SEM are shown, $^{*}P < 0.05$, $^{**}P < 0.01$, $^{***}P < 0.001$, $^{****}P < 0.0001$.

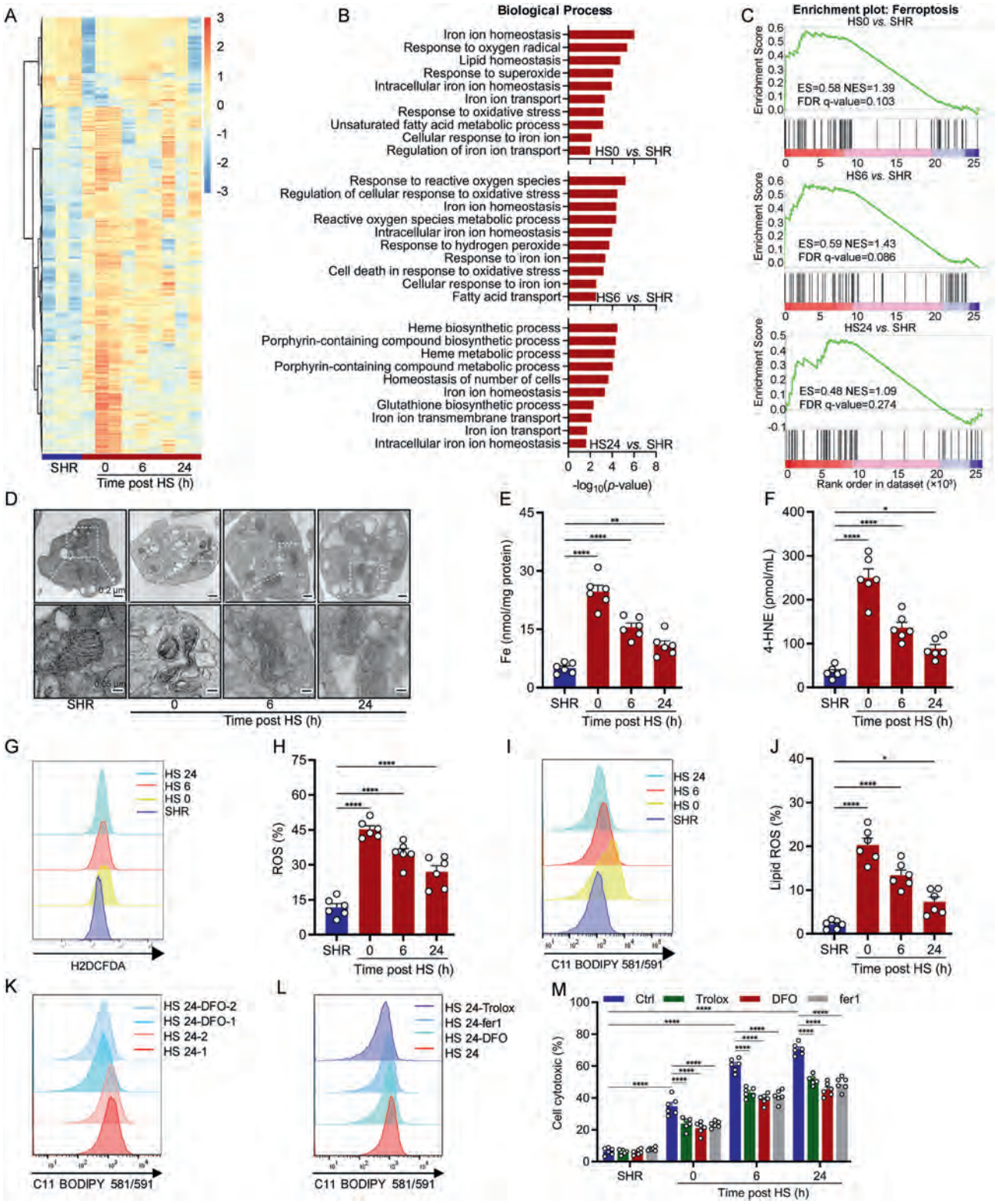

Figure 3 Ferroptosis contributes to a decrease in platelet counts in murine HS. (A) Heatmap of differentially expressed genes of platelets in SHR mice and mice at 0, 6, 24 h post-HS ($n = 3$ per group). (B) Gene ontology (GO: biological process, BP) analysis of ferroptosis-related pathway of platelets in SHR mice and mice at 0, 6, 24 h post-HS. (C) Gene Set Enrichment Analysis of platelets against SHR mice and mice at 0, 6, 24 h post-HS. (D) Representative transmission electron microscopy fields showing mouse platelet ultra-structures ($n = 3$ independent experiments per group, scale bars: 0.2 and 0.05 μm). (E, F) The level of total iron (E) in platelets and plasma 4-HNE (F) from SHR mice and mice at 0, 6, 24 h post-HS ($n = 6$ mice per group). (G–J) Flow cytometric analysis of the percentage of ROS (detected by H2DCFDA, G and H) and lipid ROS (detected by C11 BODIPY 581/591 staining, I and J) in mouse platelets between SHR and 0, 6, 24 h post-HS ($n = 6$ mice per group).

highlighting a Tfr1-dependent ferroptosis mechanism in HS. *Tfr1* overexpression in platelets of CKO-*Tfr1* mice (Fig. S9H) resulted in increased total iron (Fig. S9I), lipid ROS (Fig. S9J), and 4-HNE levels (Fig. S9K) post-HS *in vivo*, along with platelet mortality under heat stress *in vitro* (Fig. S9L), all of which could be reversed by ferroptosis inhibitors, fer1 and DFO (Fig. S9I and S9L). Taken together, these analyses suggest a fundamental role for Tfr1 in driving platelet ferroptosis under heat stress.

Tfr1 regulates intracellular iron homeostasis by mediating membrane iron transport, while post-translational modifications are involved in protein trafficking and function. The Uniprot website predicts that Tfr1 can undergo phosphorylation, palmitoylation, and glycosylation, and these modifications may be involved in the function of Tfr1. To reveal the protein modification of Tfr1, platelets were treated with phosphorylation inhibitor (staurosporine), palmitoylation inhibitor (2BP), and glycosylation inhibitor (tunicamycin or benzyl-α-GalNAc). The palmitoylation inhibitor 2BP effectively reduced total iron (Supporting Information Fig. S10A), Fe^{2+} (Fig. S10B), lipid ROS (Fig. S10C), 4-HNE (Fig. S10D), and cell mortality (Fig. S10E) levels under heat stress *in vitro*, highlighting the critical role of palmitoylation in iron uptake. Given that cellular iron uptake by Tfr1 has been linked to palmitoylation[16,17], we further employed the ABE palmitoylation assay and IEM (Fig. 4L and M) to assess the extent of palmitoylation, confirming Tfr1 palmitoylation in heat-stressed platelets, suggesting a regulatory role in transferrin-bound iron transfer. Palmitoylation is a critical, reversible post-translational protein modification mediated by zinc-finger DHHC-type containing proteins (ZDHHCs), which regulates membrane localization, stability, and protein−protein interactions[18]. RNA-seq and qPCR analysis revealed upregulation of *Zdhhc2*, a zinc finger protein involved in palmitoylation, among other *Zdhhcs* and acyl-protein thioesterases (APTs, encoded by *Lyplas* genes) post-HS (Fig. 4N, Supporting Information Fig. S11A−S11H). Co-IP analysis revealed an interaction between ZDHHC2 and Tfr1 in platelets from both SHR and HS (Fig. 4O). ABE analysis of PLPs demonstrated that knockdown or overexpression of *Zdhhc2* led to a reduction or increase in Tfr1 palmitoylation, respectively, *in vitro* (Fig. 4P). Flow cytometry analysis of holo-TF on the PLP surface further revealed that *Zdhhc2* knockdown resulted in the retention of the holo-TF membrane signal, suggesting impaired Tfr1 internalization and recycling, while *Zdhhc2* overexpression promoted Tfr1 internalization and recycling, leading to a rapid reduction or recovery of the holo-TF membrane signal post-heat stress *in vitro* (Fig. 4Q). These results indicate that palmitoylation is involved in the membrane translocation of platelet Tfr1 under heat stress conditions. Meanwhile, knockdown of *Zdhhc2* in PLPs derived from both MEG-01 cells and *Tfr1*-overexpressing MEG-01 cell lines (Fig. S11I) reduced total iron (Fig. S11J), Fe^{2+} (Fig. S11K), lipid ROS (Fig. S11L), 4-HNE (Fig. S11M), and cell cytotoxicity (Fig. S11N) *in vitro*. Conversely, *Zdhhc2* and *Tfr1* overexpression increased these levels, which were reversed by the ferroptosis inhibitor fer-1 (Fig. S11J−S11N), confirming a *Zdhhc2*-dependent mechanism in Tfr1 under heat stress. In summary, our findings implicate Tfr1 palmitoylation mediated by ZDHHC2 as a key driver in platelet ferroptosis during heat stress, offering new insights into the pathogenesis of HS and potential therapeutic targets.

3.5. Platelet-derived IL-1β amplifies liver injury in the HS murine model

GO pathway enrichment analysis highlighted the significant role of platelets in regulating the inflammatory response in HS, underscoring their function in immune modulation (Fig. 5A). Platelets store and release biologically active molecules, such as cytokines, chemokines, and eicosanoids, during activation, adhesion and aggregation[25,26]. Immunofluorescence showed platelet adhesion and aggregation in liver tissue, Kupffer cells, and hepatocytes *in vivo* and *in vitro* (Fig. 5B, Supporting Information Fig. S12A). In the HS group, the expression of P-selectin (Fig. 5C), *Cd62p* (Fig. S12B), *Cd41* (Fig. S12C), *Cd42b* (Fig. S12D) was correspondingly changed, indicating platelet activation, adhesion, and aggregation in HS. GO analysis further highlighted pathways associated with IL-4, IL-6, and IL-1 in HS platelets (Fig. 5D). To eliminate potential confounding effects from classical immune cells, mouse platelets were first purified and then exposed to heat stress *in vitro*. Inflammatory markers, including *Il1b* (Fig. 5E), *Casp1* (Fig. 5F), *Ccl5* (Fig. S12E), *Hmgb1* (Fig. S12F), *Nlrp3* (Fig. S12G), *Il1a* (Fig. S12H), *Il4* (Fig. S12I), *Il6* (Fig. S12J), and *Il18* (Fig. S12K), were significantly elevated under heat stress *in vitro*. Notably, *Il1b* and *Nlrp3* were the most striking and closely aligned with the trends observed in HS liver injury (Fig. 5E and F, Fig. S12E−S12K). IL-1β is a key pro-inflammatory cytokine activated by Caspase-1 through NLRP3 inflammasome activation, further highlighting the significant role of platelet-derived IL-1β in HS-induced liver injury. The upregulation of Caspase-1 in platelets (Fig. 5G), plasma IL-1β levels (Fig. 5I) in HS mice, and IL-1β secretion in platelet supernatants (Fig. 5H) under heat stress *in vitro*, further implicate their role in liver injury. *Tfr1* knockout or overexpression in CKO-*Tfr1* platelets, with or without ferroptosis inhibitors (fer-1 and DFO), altered the expression of Caspase-1 and IL-1β, respectively (Fig. 5G−I). *Zdhhc2* knockdown in PLPs derived from both MEG-01 cells and *Tfr1*-overexpressing MEG-01 cells decreased IL-1β levels in supernatants, whereas *Zdhhc2* overexpression increased IL-1β expression, which was reversed by the ferroptosis inhibitor fer-1 (Fig. 5J), suggesting an association between Tfr1 palmitoylation and IL-1β secretion. In addition, elevated levels of IL-6, IL-10, and TNF-α in plasma indicate the involvement of additional inflammatory factors post-HS (Fig. S12L−S12N). To summarize, our study uncovers a novel pathway in which platelet-derived inflammatory responses, particularly those induced by IL-1β, exacerbate liver injury in HS, offering new insights into the inflammatory role of platelets.

3.6. Amelioration of liver injury in the HS murine model via ferroptosis inhibition and Tfr1 ablation in platelets

To evaluate the therapeutic potential of targeting platelet ferroptosis and Tfr1 in liver injury and survival in the HS murine model,

(K) Representative flow analysis images of lipid ROS (detected by C11 BODIPY 581/591 staining) in platelets from SHR mice and mice at 0, 6, 24 h post-HS, with or without ferroptosis inhibitor DFO ($n = 3$ independent experiments). (L) Representative flow analysis images of lipid ROS (detected by C11 BODIPY 581/591 staining) with ferroptosis inhibitor Trolox, fer1, DFO in mouse platelets under heat stress *in vitro* ($n = 3$ independent experiments). (M) Cell cytotoxicity of mouse platelets was measured by LDH activity under heat stress *in vitro* ($n = 6$ independent experiments). Mean ± SEM are shown, $^{*}P < 0.05$, $^{***}P < 0.001$, $^{****}P < 0.0001$.

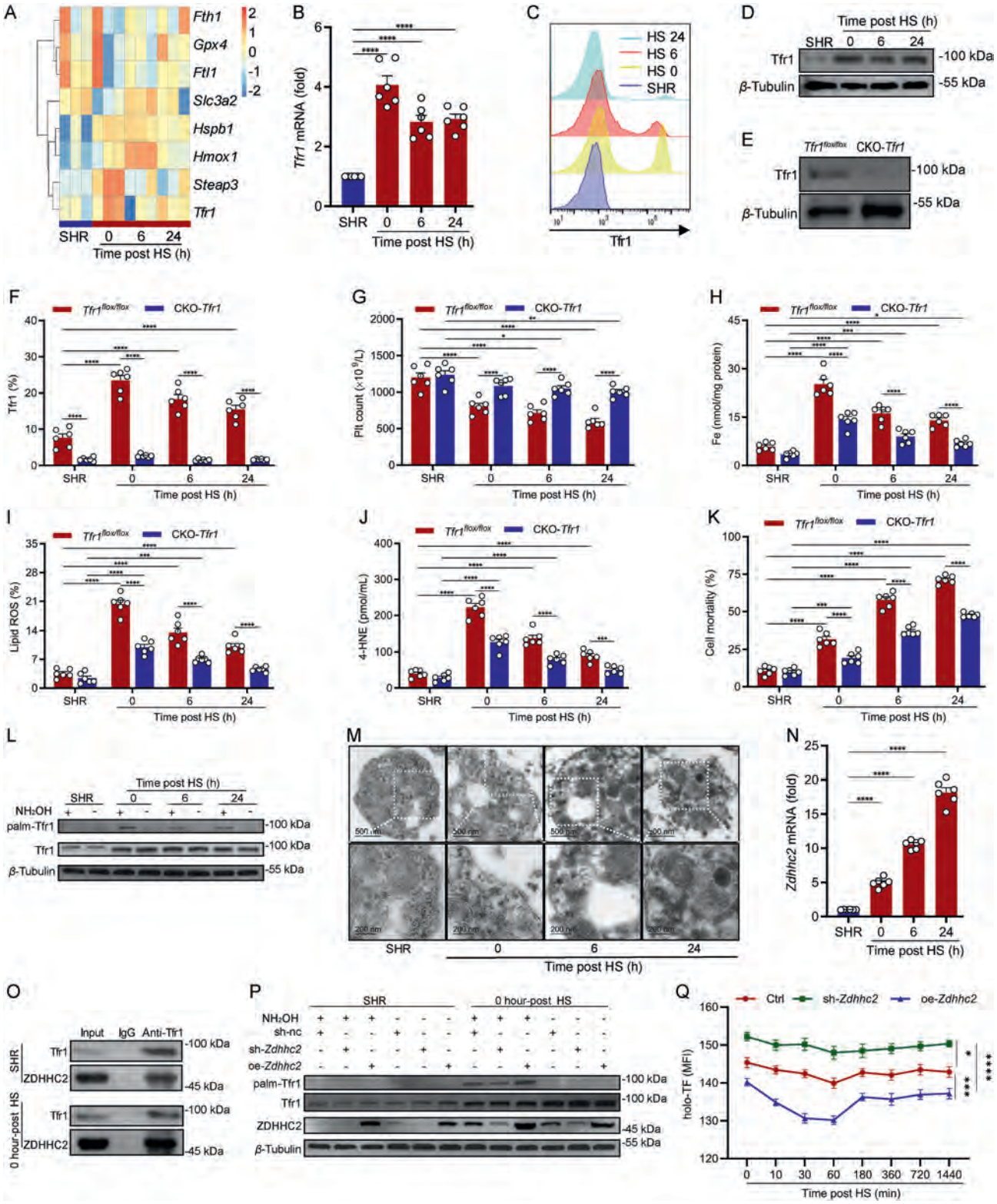

Figure 4 Identification of Tfr1 as a key mediator of platelet ferroptosis in murine HS. (A) The heatmap illustrates the expression of ferroptosis-related genes in platelets from SHR mice and mice at 0, 6, 24 h post-HS ($n = 3$ per group). (B) Expression of *Tfr1* mRNA in platelets from SHR mice and mice at 0, 6, 24 h post-HS ($n = 6$ mice per group). (C, D) Representative flow cytometric analysis (C) and Western blot (D) of platelet Tfr1 in SHR mice and mice at 0, 6, 24 h post-HS ($n = 3$ independent experiments). (E) Western blot detection of Tfr1 expression in platelets from *Tfr1*$^{flox/flox}$ and CKO-*Tfr1* mice ($n = 3$ independent experiments). (F) Flow cytometry detection of Tfr1 expression in platelets from *Tfr1*$^{flox/flox}$ and CKO-*Tfr1* mice ($n = 6$ mice per group). (G) Platelet counts over time at SHR and 0, 6, 24 h post-HS in *Tfr1*$^{flox/flox}$ and CKO-*Tfr1* mice ($n = 6$ mice per group). (H–J) The levels of total iron (H), lipid ROS (I, detected by C11 BODIPY 581/591 staining) in platelets and plasma 4-HNE (J) from *Tfr1*$^{flox/flox}$ and CKO-*Tfr1* mice before and post-HS ($n = 6$ mice per group). (K) Cell cytotoxicity (measured by LDH) of mouse platelets

platelet-specific Tfr1 conditional knockout mice (CKO-*Tfr1*), administered AAV9-DIO-*Tfr1* or Vector, were used. Vector-administered CKO-*Tfr1* significantly inhibited HS-induced thrombocytopenia (Fig. 6A), liver injury (Fig. 6B and C), and significantly improved the survival rate of mice post-HS (Fig. 6D), which could be reversed by AAV9-DIO-*Tfr1* (Fig. 6A−D). The application of ferroptosis inhibitors significantly improved the outcomes induced by AAV9-DIO-*Tfr1* (Fig. 6A−D). In addition, elevated expression levels of hepatocyte growth factor (*Hgf*), *Met*, and *Ctnnb1* were detected in HS liver tissue, indicating the activation of tissue repair and regeneration processes (Supporting Information Fig. S13A−S13C). Meanwhile, the regeneration marker Ki-67 was also found to be upregulated post-HS (Fig. S13D), indicating the activation of self-repair mechanisms to mitigate damage and facilitate liver recovery, thereby contributing to the improved condition 24 h post-HS. In summary, inhibiting ferroptosis and targeting Tfr1 in platelets are effective strategies for reducing liver injury and improving survival in HS. This approach offers a promising therapeutic avenue for intervention in HS-induced liver injury.

4. Discussion

Our investigation highlights the critical role of platelets in HS-induced liver injury, establishing a close connection between thrombocytopenia and liver injury. We discovered a Tfr1 palmitoylation-dependent ferroptosis pathway in platelets that mediates this connection. Inhibiting this pathway or ablating Tfr1 in platelets alleviates liver injury and improves prognosis, as demonstrated by our results (Fig. 7). Reduced platelet counts consistently correlated with severe liver injury in both HS patients and a murine model, suggesting platelets as potential biomarkers for HS prognosis. The liver's central role in immune responses and metabolic processes makes its vulnerability to HS-induced damage particularly evident. This study deepens our understanding of the pathophysiology of HS and paves the way for novel therapeutic interventions, emphasizing the importance of platelet count and ferroptosis mechanisms in liver injury during HS.

Clinical data from HS patients at Southern Theater General Hospital in China revealed varying severity of liver injuries, suggesting pathogenic factors beyond heat. Ultrastructural changes in liver tissues, including vascular congestion, hemorrhagic thrombosis, hepatocellular degeneration, and extensive cholestasis, indicate that amplified by ischemia−reperfusion and systemic inflammatory responses may amplify liver injury in HS[7]. Notably, liver injury in HS differs from other hepatic conditions, such as viral hepatitis, drug-induced hepatic injury, and sepsis-related liver injury. In HS, liver injury is strictly minimal in zonal necrosis and lack of fibrosis in the central area, but with pronounced swelling, hydropic change, and coagulation abnormalities[27]. Despite interventions like cooling and symptomatic support, effective treatments for HS-induced liver injury remain limited, underscoring the urgent need for research into its pathogenesis and the development of sensitive biomarkers and tailored therapeutic strategies.

Platelets, abundant in blood, are derived from bone marrow megakaryocytes and play key roles in various pathological conditions[25,28]. Consistent with our previous finding, admission platelet count is associated with mortality in HS patients[28]. In this study, the differences between HC and HS, along with dynamic changes in platelet count, were further examined. Additionally, the correlation between platelet count, organ damage, and the most platelet-affected organ in HS was explored, providing new insights into platelet dynamics under heat stress and revealing that ferroptosis-induced platelet depletion contributes to thrombocytopenia and establishes a fundamental connection with liver injury. An increased MPV and broader PDW in HS patients indicate a reduction in platelet count, coupled with the production of more active and younger platelets. Intriguingly, platelet counts were negatively correlated with markers of organ damage (*e.g.*, CTNI, ALT, AST, TBIL, SOFA, CR, and APACHE II), while positively correlated with GCS, suggesting that platelet count could serve as a key indicator of organ damage and prognosis in HS patients. The negative correlation between platelet count and critical markers such as Tc max, IL-1β, and ALT, consistent with previous studies, highlights platelet counts as a primary factor in assessing HS severity and prognosis[29]. Another notable aspect of our findings is the biological function of IL-1β, which is identified as a key mediator of HS-induced liver injury, as demonstrated in our previous study[30]. Tissue damage can trigger self-repair mechanisms. Expression of typical liver repair and regeneration markers, including hepatocyte growth factor, *Met*, *Ctnnb1*, and Ki-67[31], was increased, indicating active repair and regeneration, which led to a decrease in liver injury markers at 24 h post-HS. In conclusion, our study emphasizes the prognostic value of platelet counts in HS, suggesting that lower platelet counts are predictive of more severe organ injury and decreased survival rates.

Recent studies have broadened the understanding of platelets, highlighting their involvement in immune function and inflammatory signaling, beyond their traditional role in coagulation[26,32,33]. Platelets express multiple receptors, such as Fc receptor, complement receptor 2, leukocyte differentiation antigen, integrin, and pattern recognition receptors, especially several Toll-like receptors[34]. These receptors enable platelets to recognize pathogens, DAMPs, and immune complexes, facilitating antigen presentation[34,35]. Additionally, activated platelets can release various δ particles, Weibel-Palade bodies, adhesion molecules, and inflammatory cytokines[36]. Our results reveal that platelets can be activated, adhere, aggregate, synthesize, and secrete granule contents and cytokines, with IL-1β being particularly prominent, thereby contributing to inflammation regulation under heat stress.

under heat stress *in vitro* ($n = 6$ mice per group). (L) Acyl-Biotin exchange detection of Tfr1 palmitoylation (palm-Tfr1) level in mouse platelets from SHR mice and mice at 0, 6, 24 h post-HS, with or without NH_2OH treatment ($n = 3$ independent experiments). (M) Representative immunoelectron microscopy images for the location of Tfr1 in mouse platelets from SHR mice and mice at 0, 6, 24 h post-HS ($n = 3$ independent experiments, scale bars: 0.5 and 0.2 μm). (N) qPCR analysis of *Zdhhc2* mRNA expression in platelets from SHR mice and mice at 0, 6, 24 h post-HS ($n = 6$ independent experiments). (O) Co-IP analysis of the interaction between Tfr1 and ZDHHC2 protein in platelets from SHR and HS0 mice ($n = 3$ independent experiments). (P) Acyl-Biotin exchange was used to detect the palmitoylation level of Tfr1 in PLP from sh-*Zdhhc2* MEG-01 cells, oe-*Zdhhc2* MEG-01 cells, and MEG-01 cells under heat stress *in vitro*, with or without NH_2OH treatment ($n = 3$ independent experiments). (Q) Flow cytometric analysis of the holo-TF signal on the surface of PLP from sh-*Zdhhc2* or oe-*Zdhhc2* MEG-01 cells under heat stress *in vitro* ($n = 3$ independent experiments). Mean ± SEM are shown, $^*P < 0.05$, $^{**}P < 0.01$, $^{***}P < 0.001$, $^{****}P < 0.0001$.

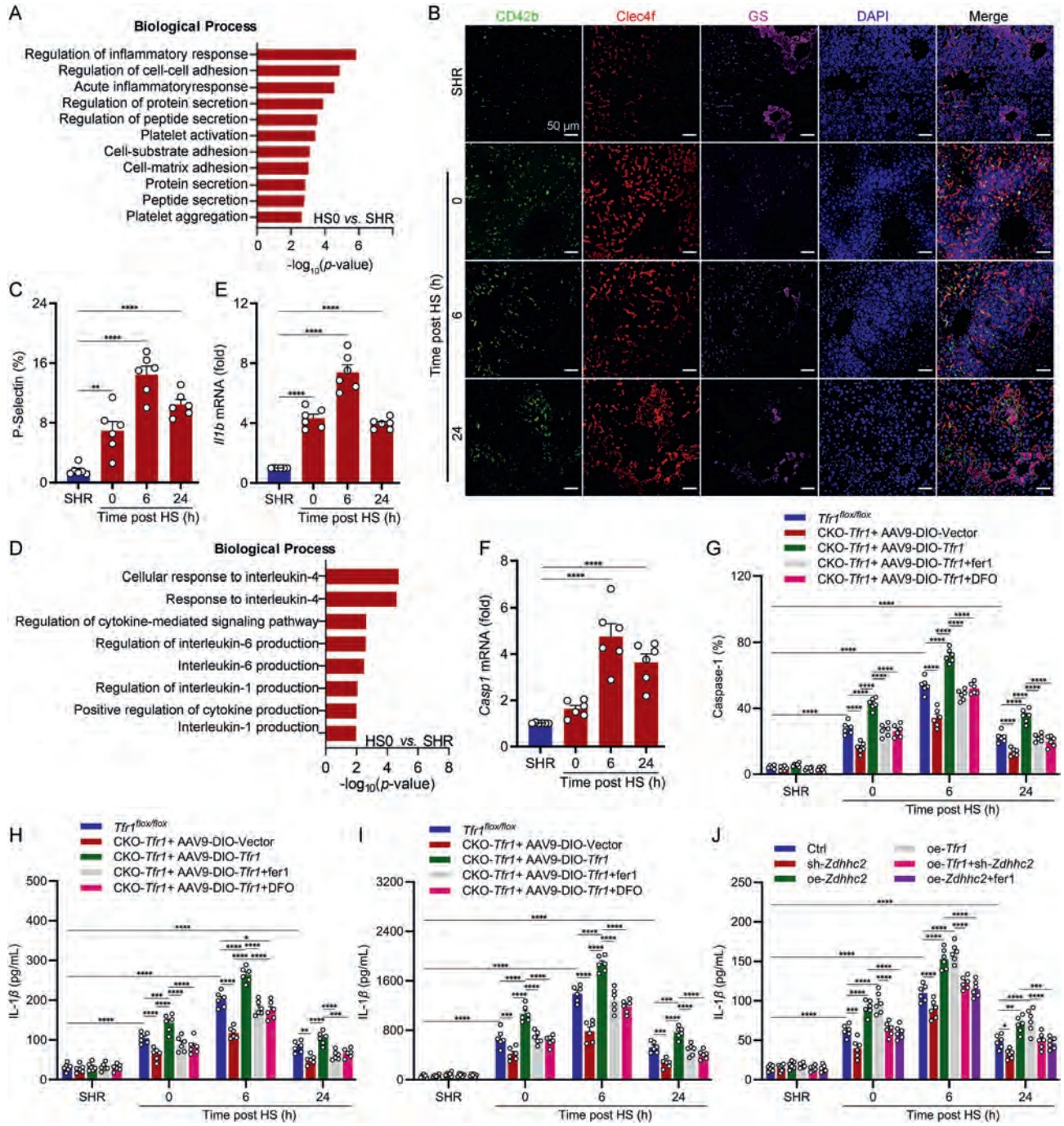

Figure 5 Platelet-derived IL-1β contributes to liver injury in the HS murine model. (A) GO (BP) analysis of the physiological and pathological states of platelets in SHR mice and mice at 0 h post-HS (HS0). (B) Representative images of immunofluorescence in liver tissue from SHR and HS mice ($n = 3$ independent experiments, scale bars, 50 μm). DAPI (blue), CD42b for platelets (green), Clec4f for Kupffer cells (red), Glutamine Synthetase (GS) for central vein zone (purple). (C) Flow cytometric analysis of the percentage of P-selectin expression on platelets in SHR mice and mice at 0, 6, 24 h post-HS ($n = 6$ mice per group). (D) GO (BP) analysis of cytokine-related pathways in platelets from SHR mice and at HS onset (HS0). (E, F) qPCR analysis of *Il1b* (E) and *Casp1* (F) mRNA expression of platelets under heat stress *in vitro* ($n = 6$ mice per group). (G) Flow cytometry analysis of caspase-1 levels in platelets from *Tfr1*$^{flox/flox}$ mice, CKO-*Tfr1* mice and CKO-*Tfr1* mice infected with AAV9-DIO-*Tfr1*, with or without ferroptosis inhibitor fer1 and DFO ($n = 6$ mice per group). (H) ELISA analysis of IL-1β levels in the supernatant of platelets under heat stress *in vitro* ($n = 6$ mice per group). (I) ELISA analysis of IL-1β levels in plasma from *Tfr1*$^{flox/flox}$ mice, CKO-*Tfr1* mice, and CKO-*Tfr1* mice infected with AAV9-DIO-*Tfr1*, with or without ferroptosis inhibitor fer1 and DFO ($n = 6$ mice per group). (J) ELISA analysis of IL-1β levels in PLP supernatant from sh-*Zdhhc2,* oe-*Zdhhc2*, oe-*Tfr1*, oe-*Tfr1*-sh-*Zdhhc2* MEG-01 cells under heat stress *in vitro*, with or without ferroptosis inhibitor fer1 ($n = 6$ independent experiments). Mean ± SEM are shown, $^{**}P < 0.01$, $^{***}P < 0.001$, $^{****}P < 0.0001$.

In liver tissues, platelets were also observed adhering to hepatocytes and Kupffer cells, undergoing shape changes, and aggregating within sinusoids. IL-1β, a key downstream mediator of the NLRP3 inflammasome, is particularly activated by DAMPs and PAMPs[37]. Its upregulation in heat-stressed platelets suggests a role in triggering the defense reaction and inflammatory response. This is further evidenced by the observed activation of NLRP3 and Caspase-1 in heat-stressed platelets. These findings align with recent studies documenting the immunomodulatory roles of anucleate platelets, including the assembly of the NLRP3 inflammasome and secretion of IL-1β in various diseases[38-42]. IL-1β could elevate body temperature, activate and recruit immune cells to the injury sites, and regulate systemic and local responses[43,44]. This not only extends our previous research into liver injury mechanisms but also underscores the complex and critical roles of platelets in inflammatory and immune responses, particularly in HS[30].

Heat stress not only reduces platelet counts but also enhances platelet cytotoxicity, potentially implicating cell death mechanisms, like ferroptosis. Ferroptosis, an iron-dependent form of cell death characterized by the accumulation of lipid peroxides in cell membranes, has been widely observed across various cell types and diseases[11]. Recent studies have reported that hemin-induced platelet activation and ferroptosis, driven by ROS, are associated with proteasome activity and inflammasome activation, proposing

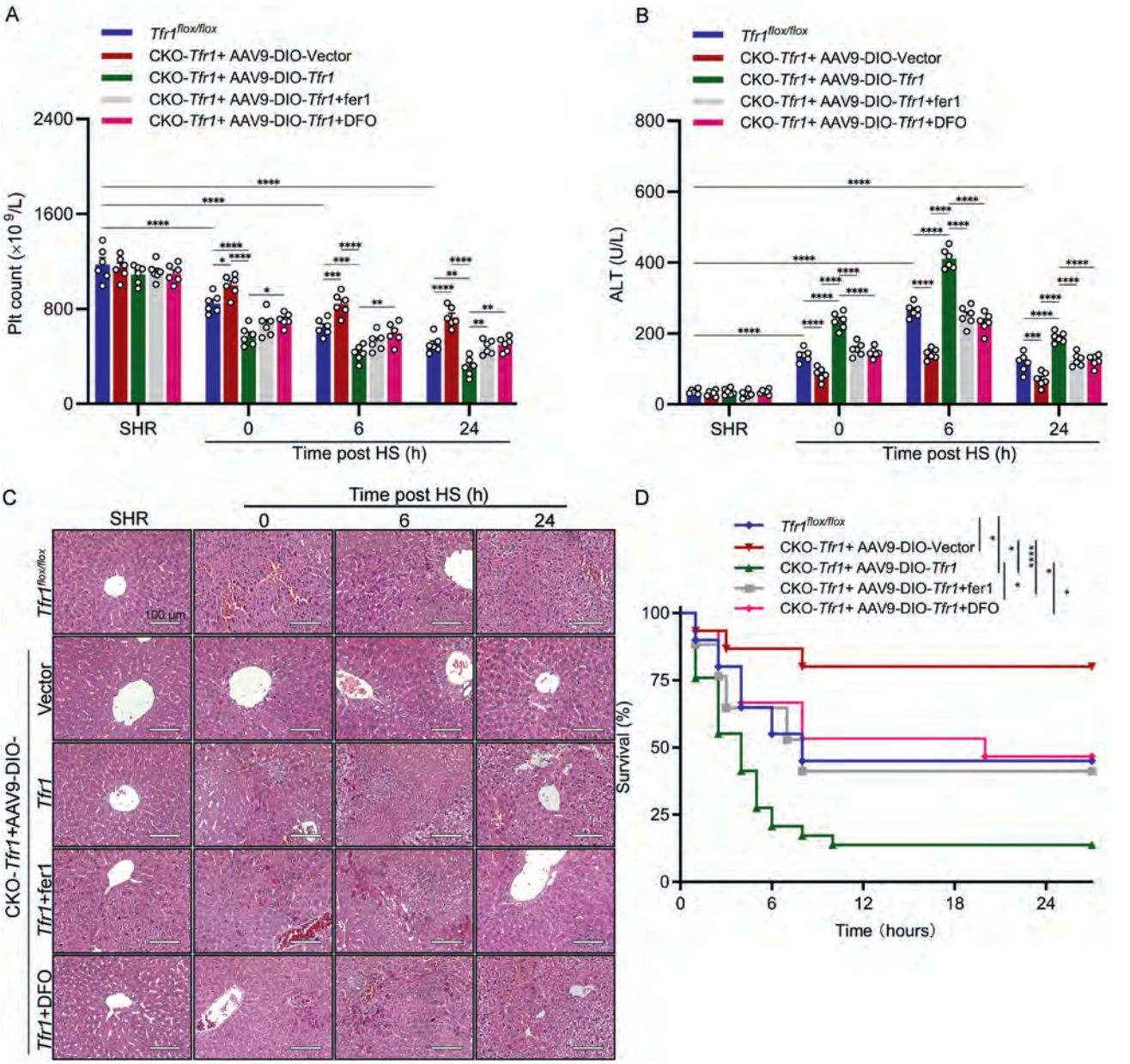

Figure 6 Amelioration of liver injury in HS murine model *via* ferroptosis inhibition and Tfr1 ablation in platelets. (A–C) Platelet count (A), plasma ALT (B), and representative HE staining images of liver tissue (C) from *Tfr1*$^{flox/flox}$ mice, and CKO-*Tfr1* mice infected with AAV9-DIO-Vector or AAV9-DIO-*Tfr1*, with or without ferroptosis inhibitor fer1 or DFO (n = 6 mice per group, scale bars: 100 μm). (D) Survival curves of mice (*Tfr1*$^{flox/flox}$ mice, n = 20; CKO-*Tfr1*+AAV9-DIO-Vector mice, n = 15; CKO-*Tfr1*+AAV9-DIO-*Tfr1* mice, n = 29; CKO-*Tfr1*+AAV9-DIO-*Tfr1*+fer1 mice, n = 17; CKO-*Tfr1*+AAV9-DIO-*Tfr1*+DFO mice, n = 15). Mean ± SEM are shown, *P < 0.05, **P < 0.01, ***P < 0.001, ****P < 0.0001.

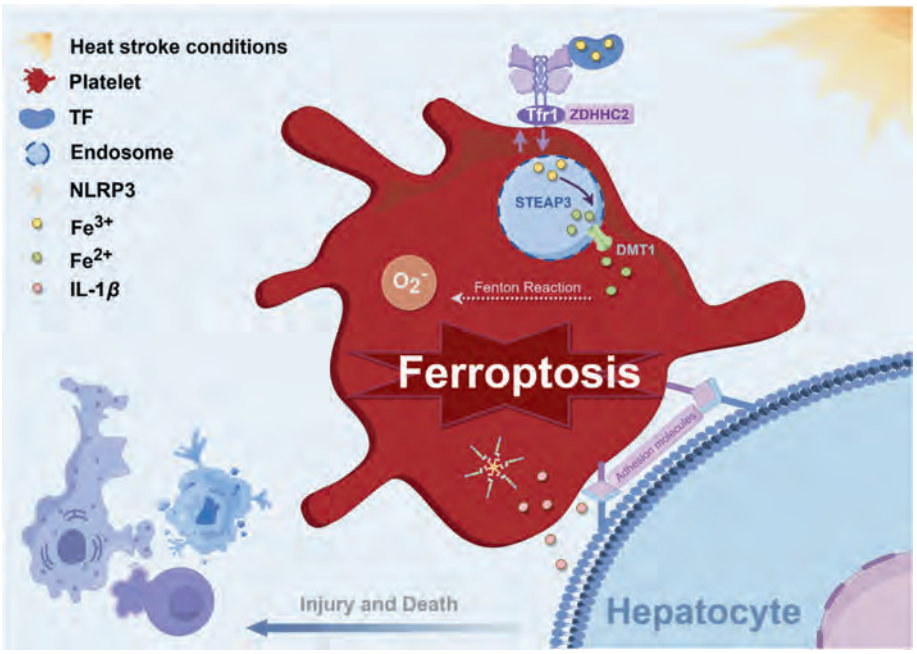

Figure 7 Tfr1 palmitoylation-mediated ferroptosis in platelets, accompanied by IL-1β secretion, exacerbates liver injury in HS. The findings provide novel insights into thrombocytopenia and liver injury in HS, offering a potential therapeutic strategy to mitigate HS-induced thrombocytopenia, liver injury, and poor prognosis.

a complex interplay between ferroptosis, inflammation, and platelet activation[45,46]. In our murine HS model, we reported, for the first time, that ferroptosis occurs in platelets *in vivo*. This was assessed by the increased expression of lipid ROS, 4-HNE, total iron, and Fe^{2+}, along with changes in mitochondrial morphology. Tfr1 is the key rate-limiting factor controlling iron uptake and acts as the driver of the ferroptosis process[13]. In the study, we discovered that platelet ferroptosis is dependent on Tfr1 palmitoylation in HS. Moreover, we also found that the expression of certain genes that inhibit ferroptosis in platelets, such as *Slc40a1* and heat shock protein B1 (*Hspb1*), increased post-HS. SLC40A1 (ferroportin), the only known mammalian iron export protein, transports Fe^{2+} out of the cell[47]. HSPB1, a member of the small heat shock protein family, is involved in cellular stress responses by aiding protein folding, preventing aggregation, stabilizing membrane structures, reducing ROS accumulation, and inhibiting lipid peroxidation[48]. Our results showed that knockdown of *Hspb1* and *Slc40a1*, particularly *Slc40a1*, led to increased total iron, Fe^{2+}, lipid ROS, 4-HNE, and cell mortality in PLPs after heat stress, suggesting that *Slc40a1* plays a role in iron export in platelets under heat stress conditions. The expression of these ferroptosis-negative regulatory genes, along with their combined effect in platelets, explains the decrease in iron and lipid peroxidation markers at 6 and 24 h post-HS. In summary, our findings highlight the critical role of Tfr1 in platelets, especially in regulating iron transport, thereby modulating lipid peroxidation and ferroptosis in HS.

Tfr1 regulates iron ion homeostasis and is known to undergo palmitoylation, a process that manages the protein's internalization and recycling[16,17]. This dynamic palmitoylation process is crucial for protein targeting and interactions within the membrane, stability, and subcellular distribution, ultimately influencing protein activity[18,49]. Our study demonstrates that Tfr1 undergoes palmitoylation in platelets, a finding supported by the ABE palmitoylation assay and IEM. This palmitoylation ensures the effective transfer of Tfr1 within the platelets, contributing to iron overload and triggering ferroptosis under heat stress conditions. Furthermore, our study aligns with previous research, which reported that the function and regulation of Tfr1 are associated with palmitoylation modification[16,17]. Interestingly, Agnès Rötig attributed the delayed Tfr1 recycling in palmitoylation defect on iron accumulation or overload diseases, whereas we tend to think the influence of palmitoylation mediated by ZDHHC2 in platelets under heat stress is dynamic and may also encompass the integration of spatial and cellular responses, not only in endocytosis, recycling, but more specifically in stabilized Tfr1, retards proteasome degradation, signaling as well as crosstalk with deacylation and other modifications, which need to be further explored[16,17]. The use of the palmitoylation inhibitor 2BP significantly reduced total iron, Fe^{2+}, lipid ROS, 4-HNE, and platelet mortality, reinforcing the link between Tfr1 palmitoylation and platelet ferroptosis. Additionally, TF-Tfr1 internalization and recycling experiments demonstrated that *Zdhhc2* is involved in the translocation of Tfr1, with a high internalization and recycling rate within the first few hours, which may explain why total iron, Fe^{2+}, ROS, lipid ROS, and 4-HNE peaked at 0 h post-HS. However, *Zdhhc2* (along with other palmitoylation-related enzymes) remained elevated at 6 and 24 h post-HS, indicating a sustained demand for palmitoylation in platelets. This further suggests that *Zdhhc2*-mediated palmitoylation of Tfr1 serves as a key regulatory mechanism in platelet ferroptosis. Inhibiting Tfr1-dependent ferroptosis in platelets not only preserves platelet counts but also reduces IL-1β production, thereby mitigating liver damage and improving survival in HS.

5. Conclusions

In summary, the current investigation uncovers a novel mechanistic pathway in HS, where Tfr1-palmitoylation-dependent

ferroptosis in platelets plays a crucial role, offering new therapeutic targets to mitigate HS-induced liver injury.

Acknowledgments

This study was funded by the National Natural Science Foundation of China (grant Nos. 82471912 and 82072436, China), Guangdong Basic and Applied Basic Research Foundation (2025A1515012449, China), and the Provincial Key Laboratory of Immune Regulation and Immunotherapy (2022B1212010009, China). The authors gratefully acknowledge the contributions of all the investigators of the program. A schematic diagram was prepared by Figdraw (www.figdraw.com).

Author contributions

Qiyuan An: Writing − original draft, Visualization, Validation, Methodology, Data curation. Riqing Wei: Validation, Methodology. Zhicheng Huang: Visualization, Methodology, Investigation, Data curation. Youyong Tang: Methodology, Investigation, Data curation. Minghao Wang: Investigation, Formal analysis, Data curation. Sixiao He: Investigation, Formal analysis, Data curation. Kaihua Huang: Investigation, Formal analysis, Data curation. Zhifeng Liu: Investigation, Formal analysis, Data curation. Meimei Zhang: Investigation, Formal analysis. Ru Li: Methodology. Junhao Huang: Investigation. Keying Zhang: Investigation. Jingjing Ji: Data curation. Liwei Xie: Writing − review & editing, Visualization, Supervision, Project administration, Investigation, Funding acquisition. Qiang Ma: Writing − review & editing, Supervision, Funding acquisition.

Conflicts of interest

The authors declare no competing interests.

Appendix A. Supplementary information

Supporting Information to this article can be found online at https://doi.org/10.1016/j.apsb.2025.10.027.

References

1. Wang F, Zhang Y, Li J, Xia H, Zhang D, Yao S. The pathogenesis and therapeutic strategies of heat stroke-induced liver injury. *Crit Care* 2022;**26**:391.
2. Krenkel O, Tacke F. Liver macrophages in tissue homeostasis and disease. *Nat Rev Immunol* 2017;**17**:306−21.
3. Slaba I, Wang J, Kolaczkowska E, McDonald B, Lee WY, Kubes P. Imaging the dynamic platelet-neutrophil response in sterile liver injury and repair in mice. *Hepatology* 2015;**62**:1593−605.
4. Wong CH, Jenne CN, Petri B, Chrobok NL, Kubes P. Nucleation of platelets with blood-borne pathogens on kupffer cells precedes other innate immunity and contributes to bacterial clearance. *Nat Immunol* 2013;**14**:785−92.
5. Hobisch-Hagen P, Jelkmann W, Mayr A, Wiedermann FJ, Fries D, Herold M, et al. Low platelet count and elevated serum thrombopoietin after severe trauma. *Eur J Haematol* 2000;**64**:157−63.
6. Schiodt FV, Balko J, Schilsky M, Harrison ME, Thornton A, Lee WM, et al. Thrombopoietin in acute liver failure. *Hepatology* 2003;**37**: 558−61.
7. Kew MC, Minick OT, Bahu RM, Stein RJ, Kent G. Ultrastructural changes in the liver in heatstroke. *Am J Pathol* 1978;**90**:609−18.
8. Yuan F, Cai J, Wu J, Tang Y, Zhao K, Liang F, et al. Z-DNA binding protein 1 promotes heatstroke-induced cell death. *Science* 2022;**376**: 609−15.
9. Zhang M, Zhu X, Tong H, Lou A, Li Y, Li Y, et al. Ave 0991 attenuates pyroptosis and liver damage after heatstroke by inhibiting the ROS−NLRP3 inflammatory signalling pathway. *BioMed Res Int* 2019; **2019**:1806234.
10. Huang W, Xie W, Zhong H, Cai S, Huang Q, Liu Y, et al. Cytosolic p53 inhibits parkin-mediated mitophagy and promotes acute liver injury induced by heat stroke. *Front Immunol* 2022;**13**:859231.
11. Jiang X, Stockwell BR, Conrad M. Ferroptosis: mechanisms, biology and role in disease. *Nat Rev Mol Cell Biol* 2021;**22**:266−82.
12. Li R, Wei R, Liu C, Zhang K, He S, Liu Z, et al. Heme oxygenase 1-mediated ferroptosis in Kupffer cells initiates liver injury during heat stroke. *Acta Pharm Sin B* 2024;**14**:3983−4000.
13. Kawabata H. Transferrin and transferrin receptors update. *Free Radic Biol Med* 2019;**133**:46−54.
14. Chen J, Li X, Ge C, Min J, Wang F. The multifaceted role of ferroptosis in liver disease. *Cell Death Differ* 2022;**29**:467−80.
15. Alvarez E, Girones N, Davis RJ. Inhibition of the receptor-mediated endocytosis of diferric transferrin is associated with the covalent modification of the transferrin receptor with palmitic acid. *J Biol Chem* 1990;**265**:16644−55.
16. Petit F, Drecourt A, Dussiot M, Zangarelli C, Hermine O, Munnich A, et al. Defective palmitoylation of transferrin receptor triggers iron overload in Friedreich ataxia fibroblasts. *Blood* 2021;**137**:2090−102.
17. Drecourt A, Babdor J, Dussiot M, Petit F, Goudin N, Garfa-Traore M, et al. Impaired transferrin receptor palmitoylation and recycling in neurodegeneration with brain iron accumulation. *Am J Hum Genet* 2018;**102**:266−77.
18. F SM, Abrami L, Linder ME, Bamji SX, Dickinson BC, van der Goot FG. Mechanisms and functions of protein *S*-acylation. *Nat Rev Mol Cell Biol* 2024;**25**:488−509.
19. Zhong L, Wu M, Ji J, Wang C, Liu Z. Association between platelet levels on admission and 90-day mortality in patients with exertional heatstroke, a 10 years cohort study. *Front Med* 2021;**8**:716058.
20. Tiedt R, Schomber T, Hao-Shen H, Skoda RC. Pf4-cre transgenic mice allow the generation of lineage-restricted gene knockouts for studying megakaryocyte and platelet function *in vivo*. *Blood* 2007;**109**: 1503−6.
21. Chen AC, Donovan A, Ned-Sykes R, Andrews NC. Noncanonical role of transferrin receptor 1 is essential for intestinal homeostasis. *Proc Natl Acad Sci U S A* 2015;**112**:11714−9.
22. Challis RC, Ravindra Kumar S, Chan KY, Challis C, Beadle K, Jang MJ, et al. Systemic AAV vectors for widespread and targeted gene delivery in rodents. *Nat Protoc* 2019;**14**:379−414.
23. Li J, Pan X, Pan G, Song Z, He Y, Zhang S, et al. Transferrin receptor 1 regulates thermogenic capacity and cell fate in brown/beige adipocytes. *Adv Sci (Weinh)* 2020;**7**:1903366.
24. Liu B, Liu Y, Xu S, Wu Q, Wu D, Zhan L, et al. Easymultiprofiler: an efficient multi-omics data integration and analysis workflow for microbiome research. *Sci China Life Sci* 2025. Available from: https://doi.org/10.1007/s11427-025-3035-0.
25. Semple JW, Italiano Jr JE, Freedman J. Platelets and the immune continuum. *Nat Rev Immunol* 2011;**11**:264−74.
26. Iba T, Helms J, Levi M, Levy JH. Thromboinflammation in acute injury: infections, heatstroke, and trauma. *J Thromb Haemostasis* 2024;**22**:7−22.
27. Bianchi L, Ohnacker H, Beck K, Zimmerli-Ning M. Liver damage in heatstroke and its regression. A biopsy study. *Hum Pathol* 1972;**3**: 237−48.
28. Grozovsky R, Giannini S, Falet H, Hoffmeister KM. Regulating billions of blood platelets: glycans and beyond. *Blood* 2015;**126**: 1877−84.
29. Proctor EA, Dineen SM, Van Nostrand SC, Kuhn MK, Barrett CD, Brubaker DK, et al. Coagulopathy signature precedes and predicts severity of end-organ heat stroke pathology in a mouse model. *J Thromb Haemostasis* 2020;**18**:1900−10.

30. Geng Y, Ma Q, Liu YN, Peng N, Yuan FF, Li XG, et al. Heatstroke induces liver injury *via* IL-1β and HMGB1-induced pyroptosis. *J Hepatol* 2015;**63**:622−33.
31. Ma X, Huang T, Chen X, Li Q, Liao M, Fu L, et al. Molecular mechanisms in liver repair and regeneration: from physiology to therapeutics. *Signal Transduct Targeted Ther* 2025;**10**:63.
32. Zhang J, Luo Q, Hu Q, Zhang T, Shi J, Kong L, et al. An injectable bioactive dressing based on platelet-rich plasma and nanoclay: sustained release of deferoxamine to accelerate chronic wound healing. *Acta Pharm Sin B* 2023;**13**:4318−36.
33. Tang M, Zhang Z, Wang P, Zhao F, Miao L, Wang Y, et al. Advancements in precision nanomedicine design targeting the anoikis-platelet interface of circulating tumor cells. *Acta Pharm Sin B* 2024;**14**:3457−75.
34. Koupenova M, Livada AC, Morrell CN. Platelet and megakaryocyte roles in innate and adaptive immunity. *Circ Res* 2022;**130**: 288−308.
35. Weyrich AS, Lindemann S, Zimmerman GA. The evolving role of platelets in inflammation. *J Thromb Haemostasis* 2003;**1**:1897−905.
36. Morrell CN, Aggrey AA, Chapman LM, Modjeski KL. Emerging roles for platelets as immune and inflammatory cells. *Blood* 2014;**123**: 2759−67.
37. Tschopp J, Schroder K. Nlrp3 inflammasome activation: the convergence of multiple signalling pathways on ros production?. *Nat Rev Immunol* 2010;**10**:210−5.
38. Iba T, Helms J, Levi M, Levy JH. The role of platelets in heat-related illness and heat-induced coagulopathy. *Thromb Res* 2023;**231**: 152−8.
39. Hottz ED, Lopes JF, Freitas C, Valls-de-Souza R, Oliveira MF, Bozza MT, et al. Platelets mediate increased endothelium permeability in dengue through NLRP3-inflammasome activation. *Blood* 2013;**122**: 3405−14.
40. Cornelius DC, Baik CH, Travis OK, White DL, Young CM, Austin Pierce W, et al. NLRP3 inflammasome activation in platelets in response to sepsis. *Phys Rep* 2019;**7**:e14073.
41. Vogel S, Arora T, Wang X, Mendelsohn L, Nichols J, Allen D, et al. The platelet NLRP3 inflammasome is upregulated in sickle cell disease *via* HMGB1/TLR4 and Bruton tyrosine kinase. *Blood Adv* 2018;**2**:2672−80.
42. Lindemann S, Tolley ND, Dixon DA, McIntyre TM, Prescott SM, Zimmerman GA, et al. Activated platelets mediate inflammatory signaling by regulated interleukin 1beta synthesis. *J Cell Biol* 2001; **154**:485−90.
43. Mota CMD, Madden CJ. Neural circuits mediating circulating interleukin-1β-evoked fever in the absence of prostaglandin E2 production. *Brain Behav Immun* 2022;**103**:109−21.
44. Pyrillou K, Burzynski LC, Clarke MCH. Alternative pathways of IL-1 activation, and its role in health and disease. *Front Immunol* 2020;**11**: 613170.
45. NaveenKumar SK, SharathBabu BN, Hemshekhar M, Kemparaju K, Girish KS, Mugesh G. The role of reactive oxygen species and ferroptosis in heme-mediated activation of human platelets. *ACS Chem Biol* 2018;**13**:1996−2002.
46. NaveenKumar SK, Hemshekhar M, Kemparaju K, Girish KS. Hemin-induced platelet activation and ferroptosis is mediated through ROS-driven proteasomal activity and inflammasome activation: protection by melatonin. *Biochim Biophys Acta Mol Basis Dis* 2019;**1865**:2303−16.
47. McKie AT, Barlow DJ. The SLC40 basolateral iron transporter family (ireg1/ferroportin/mtp1). *Pflügers Archiv* 2004;**447**:801−6.
48. Richter K, Haslbeck M, Buchner J. The heat shock response: life on the verge of death. *Mol Cell* 2010;**40**:253−66.
49. Dowal L, Yang W, Freeman MR, Steen H, Flaumenhaft R. Proteomic analysis of palmitoylated platelet proteins. *Blood* 2011;**118**: e62−73.